

The star-forming progenitors of massive red galaxies

A. Cattaneo^{1*}, J. Woo², A. Dekel², S. M. Faber³

¹*Laboratoire d'Astrophysique de Marseille, UMR 6110 CNRS, Univ. d'Aix-Marseille, 38 rue F. Joliot-Curie, 13388 Marseille cedex 13, France*

²*Racah Institute of Physics, The Hebrew University, Jerusalem 91904, Israel*

³*UCO/Lick Observatory, University of California, USA*

* *andrea.cattaneo@oamp.fr*

31 December 2021

ABSTRACT

The link between massive red galaxies in the local Universe and star-forming galaxies at high redshift is investigated with a semi-analytic model that has proven successful in many ways, e.g. explaining the galaxy colour-magnitude bimodality and the stellar mass-age relation for red-sequence galaxies. The model is used to explore the processes that drive star formation in different types of galaxies as a function of stellar mass and redshift. We find that most $z = 2 - 4$ star-forming galaxies with $M_* > 10^{10} M_\odot$ evolve into red-sequence galaxies. Also, most of the massive galaxies on the red-sequence today have passed through a phase of intense star formation at $z > 2$. Specifically, $\sim 90\%$ of today's red galaxies with $M_* > 10^{11} M_\odot$ were fed during this phase by cold streams including minor mergers. Gas-rich major mergers are rare and the effects of merger-driven starbursts are ephemeral. On the other hand, major mergers are important in powering the most extreme starbursts. Gas-rich mergers also explain the tail of intermediate-mass red galaxies that form relatively late, after the epoch of peak star formation. In two thirds of the currently red galaxies that had an intense star formation event at $z < 1$, this event was triggered by a merger.

Key words: galaxies: ellipticals — galaxies: evolution — galaxies: formation — galaxies: high-redshift — galaxies: starbursts

1 INTRODUCTION

Sub-mm observations have uncovered a new population of high- z star-forming galaxies (SFGs), which are detected through the far-infrared emission of dust heated by UV-bright newborn stars (Smail et al. 1997; Eales et al. 1999). These lie along a sequence in the star formation rate (SFR)-stellar mass plane that is elevated with respect to the $z = 0$ relation (Noeske et al. 2007b; Elbaz et al. 2011).

In the local Universe, ultraluminous infrared galaxies (ULIRGs), whose SFRs are several times higher than local SFGs of the same mass, are directly linked to mergers (Sanders et al. 1986). Hydrodynamic simulations reproduce this observational finding (Mihos & Hernquist 1994; Barnes & Hernquist 1991; Mihos & Hernquist 1996). The same simulations also find that the morphological properties of the remnant of gas-rich mergers are consistent with those of L_* ellipticals (Barnes & Hernquist 1996; Cox et al. 2006). These observational and theoretical results have been used to support the merger scenario, in which elliptical galaxies are formed by mergers of spirals (Toomre & Toomre 1972; Hopkins et al. 2006). In this scenario, ULIRGs correspond to the formation of elliptical galaxies caught in the act.

Massive red galaxies (i.e., Es and S0s) formed the bulk

of their stars at high z (Thomas et al. 2005), where conditions were different from the local Universe. Therefore, it is not straightforward to generalise the lesson from local ULIRGs to higher redshifts. However, progress in astronomical instrumentation has made it possible to observe the morphologies and kinematics of the high- z counterparts of ULIRGs. They are galaxies that are detected in the sub-mm and that form stars at rates of hundreds of solar masses per year. We refer to high- z ULIRGs as sub-mm galaxies (SMGs), independently of their actual sub-mm fluxes.

Engel et al. (2010) have used CO interferometric data to conclude that most bright ($L_{\text{IR}} > 5 \times 10^{12} L_\odot$) SMGs are major mergers. Förster Schreiber et al. (2009) have observed a larger sample of less extreme objects with integral field spectroscopy. They have found that only one third of their galaxies are interacting or merging. Another one third are rotation-dominated turbulent discs and the rest are velocity-dispersion-dominated objects. Kartaltepe et al. (2011) present further evidence that the highest-SFR galaxies tend to be highly disturbed even at $z \sim 2$.

These observations have a natural explanation in a scenario in which cold streams in massive haloes are the main mode of galaxy mass accretion (Kereš et al. 2005;

Dekel & Birnboim 2006). The cosmological simulations and theoretical analysis of Dekel et al. (2009) show that only one third of the stream mass is in clumps leading to mergers of mass ratios greater than 1:10. The rest is in smoother flows that preserve the disc's rotation. However, discs formed by fast accretion of cold streams are turbulent and violently unstable. They break into clumps that coalesce into a central spheroid, hence providing an alternative to the merger scenario for the formation of spheroids (Elmegreen et al. 2008). Dekel et al. (2009) find that most ($\sim 3/4$) high- z SFGs are stream-fed and that mergers are only necessary to explain the brightest SMGs, the latter being the highest-SFR subclass within SFGs.

The question is which of these two types of objects are the progenitors of $z = 0$ massive red galaxies, and conversely, how many $z = 0$ massive red galaxies have such progenitors. We should also like to know what proportion of high- z SFG's ultimately turn into massive red galaxies. In this article, we address these questions with a semi-analytic model that has proved successful in explaining local data, such as the galaxy colour - magnitude distribution in the Sloan Digital Sky Survey (Cattaneo et al. 2006) and the stellar mass - age relation for red-sequence galaxies (Cattaneo et al. 2008). The key feature that makes the model successful is inclusion of multiple mechanisms (explained below) whereby star formation can be quenched in SFGs, causing them to move to the red sequence. The model thus provides a plausible laboratory in which the importance of various gas accretion and quenching mechanisms for different types of galaxies can be compared with one another.

In this paper, the model is used both to evolve the properties of high- z SFGs to low z and to trace the progenitors of today's massive red galaxies back in time. It is necessary to analyze the problem both ways because even if all high redshift galaxies of one type evolved into massive red galaxies, that would not imply that all massive red galaxies derived from that type of object. We shall also see how the model can be used to separate stream-fed and merger-driven star formation.

It is straightforward to evolve galaxies from a given z to $z = 0$, once a semi-analytic model is given. It is trickier to tell what type of object are the progenitors of the local population of massive red galaxies because the properties of the progenitors of massive red galaxies are time-dependent. The main progenitor of a $z = 0$ elliptical may be a clumpy disc at $z = 4$, a major gas-rich merger at $z = 3$, and a massive red object at $z = 2$.

We resolve this ambiguity by introducing the redshift z_{peak} at which the star formation rate (SFR) of a galaxy's main progenitor has an absolute maximum. Stream-fed star formation is much more continuous than merger-driven star formation. If it dominates at z_{peak} , it dominates at all times. In this case, star formation is unambiguously stream-fed. The problem is more complicated when the peak SFR is linked to a merger event. In that case, we need to investigate the event's contribution to the build-up of the final stellar mass.

The plan of this work is thus as follows. In Section 2, we recall the main assumptions of the GalICS semi-analytic model used for this work. Our goal is not to give a detailed description of the GalICS model (it can be found in Hatton et al. 2003 and Cattaneo et al. 2006). It is rather to

make clear how we separate stream-fed and merger-driven star formation. We shall see that, in our model, stream-fed gas accretion and minor merger contribute to both disc star formation (directly) and bulge star formation (indirectly, by triggering disc instabilities), while major mergers only contribute the triggering of bulge star formation. Therefore, the relative importance of bulge star formation can be used to put an upper limit to the importance of major mergers in the star formation histories of galaxies. In Section 3, we describe how we assign a galaxy descendent population to a parent one, and vice versa. In Section 4, we present the mass - SFR relation at $z = 2, 3, 4$, and we discuss which subset of the galaxies that populate this relation ends up on the red sequence at $z = 0$. In Section 5, we discuss the progenitors of massive red galaxies, show some characteristic SFR histories, and describe how the properties at z_{peak} (z_{peak} , SFR_{peak}, driving mechanism) depend on a galaxy's stellar mass at $z = 0$. Section 6 presents the conclusions of the article.

2 THE GALAXY FORMATION MODEL

GalICS (Galaxies In Cosmological Simulations; Hatton et al. 2003) is a method to simulate the formation of galaxies in a Λ CDM Universe. It combines cosmological N-body simulations of the gravitational clustering of the dark matter with a semi-analytic (SAM) approach to the physics of the baryons (gas accretion, galaxy mergers, star formation and feedback).

The version of GalICS used here is the same as the 'new model' introduced in Cattaneo et al. (2006) and Cattaneo et al. (2008) and uses the same parameter values. We now recall its fundamental assumptions. We concentrate on the points that are relevant for this work and refer to the articles above for a more detailed description.

2.1 Dark-matter simulation

The cosmological N-body simulation that follows the hierarchical clustering of the dark-matter component was carried out with a parallel tree code. It assumes a flat Λ CDM Universe with a cosmological constant of $\Omega_{\Lambda} = 0.667$ and a Hubble constant of $H_0 = 66.7 \text{ km s}^{-1}$. The Λ CDM power spectrum of initial fluctuations is normalized to $\sigma_8 = 0.88$. The computational volume is a cube of size $(150 \text{ Mpc})^3$ with 256^3 particles of $8.3 \times 10^9 M_{\odot}$ each and a smoothing length of 29.3 kpc. The simulation produced 100 output snapshots spaced logarithmically in expansion factor $(1+z)^{-1}$ from $z = 35.59$ to $z = 0$.

Each snapshot was analysed with a friends-of-friends algorithm (Davis et al. 1985) to identify virialized haloes containing more than 20 particles. The minimum halo mass is thus $1.65 \times 10^{11} M_{\odot}$.

Merger trees are constructed by linking the haloes identified in each snapshot with their progenitors in the previous snapshot, i.e., all predecessors from which the halo has inherited one or more particles.

2.2 Disc formation at the centre of dark-matter haloes

The baryons in each halo are assumed to cool efficiently, i.e. to stream cold, onto the central galaxy until the dark matter halo reaches a critical mass of

$$M_{\text{crit}} = M_{\text{shock}} \times \max\{1, 10^{1.3(z-z_c)}\}. \quad (1)$$

This assumption has a simple physical justification. Above a critical halo mass of $M_{\text{shock}} \sim 10^{12} M_{\odot}$, the gas that streams into the halo is shock heated (Dekel & Birnboim 2006) and becomes vulnerable to black-hole heating, which prevents it from cooling down again (see Cattaneo et al. 2009 for a review; also see Dekel & Birnboim 2008 and Khochfar & Ostriker 2008 for a discussion of the contribution of gravitational heating).

The effects of changing M_{crit} have been studied quantitatively in Cattaneo et al. (2006), where we have shown that the value of this parameter is constrained within a factor of two.

The term $\propto 10^{1.3z}$ was introduced to account for the more efficient penetration of cold streams in massive haloes at high redshift (see Dekel & Birnboim 2006 and Dekel et al. 2009).

In Cattaneo et al. (2006), we set the model parameters to $M_{\text{shock}} = 2 \times 10^{12} M_{\odot}$ by fitting the colour-magnitude distribution in the Sloan Digital Sky Survey and to $z_c = 3.2$ by fitting the Lyman-break galaxy luminosity function at $z \simeq 3$. The gas that falls to the centre settles into a disc. Star formation is activated when the gas surface density is $\Sigma_{\text{gas}} > 10^{20} \text{ H cm}^{-2} \simeq 1 M_{\odot} \text{ pc}^{-2}$. The star formation rate is described by the star formation law:

$$\dot{M}_{\text{star}} = \frac{M_{\text{cold}}}{\beta_* t_{\text{dyn}}} (1+z)^{\alpha_*}, \quad (2)$$

where M_{cold} is the mass of cold star-forming gas and t_{dyn} is the half-rotation time at the disc's half-mass radius (determined assuming angular momentum conservation and an exponential profile). The free parameters $\beta = 50$ and $\alpha = 0.6$ were fixed by fitting the Kennicutt law (see Guiderdoni et al. 1998) and the luminosity function of Lyman-break galaxies, respectively. It is important to be aware that our predictions for the luminosity function of Lyman-break galaxies at $z \simeq 3$ are highly sensitive to our dust extinction calculations, which contain large uncertainties, and that these uncertainties trickle down in the best-fit values for both α and z_c .

In a recent article, Krumholz et al. (2012) studied how Eq. (2), which is equivalent to the Kennicutt law for local discs, extrapolates to high-redshift discs and starburst. They found that Eq. (2) applies to all galaxy types and at all redshifts with $\alpha_* \sim 0$ if t_{dyn} is the *local* freefall time. However, if t_{dyn} is the *global* dynamical time, i.e. the half-rotation time, then Eq. (2) extends to high-redshift discs, but underestimates the SFR for both low- and high-redshift starbursts. Therefore, the local freefall time is a better estimator of the star formation timescale than the global dynamical time. However, in our model we are obliged to use the global time because our model does not consider the vertical structure of galactic discs, which is important for the local freefall time.

As Eq. (2) with $\alpha_* \sim 0$ extends reasonably well to high- z galaxies classified as discs, one may argue that there is no ground for allowing $\alpha_* > 0$. However, if many of the high- z

galaxies classified as starbursts are starbursting discs (very much like the local galaxy M82), then there is indeed a case to do so. In that case, boosting the mean star-formation efficiency of discs at high z would be a way to account for the fact that, at high z , a much greater fraction of the disc population is in a starbursting rather than a quiescent mode. Notice, however, that, for $\alpha = 0.6$, the term $(1+z)^{\alpha}$ boosts the SFRs at $z \sim 3$ by little more than a factor of two, and that this is less than the precision with which the normalisation of the Kennicutt law can be determined at high z . In the Discussion, we shall consider how the uncertainty on z_c and α_* may affect the conclusions of the article.

As smooth gas accretion is the only mechanism through which discs are allowed to acquire gas, disc star formation is always stream-fed star formation. This point will be of great importance for the interpretation of our results.

2.3 Bulges

In GalICS, bulges are formed by two mechanisms: mergers and violent disc instabilities.

Bulge growth via disc instabilities is modelled by assuming that the bulge mass increases until it is sufficiently large to stabilize the disc. The stability criterion is

$$\sqrt{\frac{0.5GM_{\text{disc}}}{r_{1/2}}} < \eta \sqrt{\frac{GM(r_{1/2})}{r_{1/2}}}, \quad (3)$$

where M_{disc} is the disc mass, $r_{1/2}$ is the exponential disc's half-mass radius, $M(r_{1/2})$ is the total mass within the disc half-mass radius, and η is a parameter that controls the instability threshold (see e.g. van den Bosch 1998). This criterion translates into the condition

$$\sqrt{0.5M_{\text{disc}}} < \eta \sqrt{0.5M_{\text{disc}} + M_{\text{bulge}} + M_{\text{dm}}(r_{1/2})}, \quad (4)$$

where $M_{\text{dm}}(r_{1/2})$ is the mass of the dark matter within the disc's half-mass radius. The instability threshold is set to $\eta = 0.7$, as in Hatton et al. (2003). For this value of η , blue galaxies have bulges, yet they remain largely disc-dominated objects. The influence of the η parameter on our results will be discussed in Section 6 (Discussion and Conclusion).

Eq. (4) implies that, in the absence of mergers, the growth of the bulge is directly linked to the growth of the disc. Since bulges formed by violent disc instabilities never dominate the total galaxy mass in our model, bulge star formation triggered by disc instabilities is always secondary with respect to disc star formation. This is true irrespective of the star formation law. Even if bulge star formation happens on a much shorter timescale than disc star formation (see below), gas cannot be converted into stars faster than it is supplied to the bulge. In a context where the bulge gas accretion rate is more or less proportional but always lower than the disc gas accretion rate, disc star formation is bound to be dominant.

In GalICS, galaxy mergers are mainly due to orbital decay of satellite galaxies through dynamical friction after halo mergers have resulted in the formation of galaxy groups and clusters. The fraction of the disc that is transferred to the bulge in a merger grows with the mass ratio of the merging galaxies. It ranges from zero for a very minor merger to unity for an equal mass merger, which means that bulge formation is essentially linked to major mergers. The bulge

that forms is assumed to have a Hernquist (1990) profile and its radius is determined based on an energy conservation argument. This simplified picture of the dynamics of morphological transformations is, nevertheless, consistent with key observational constraints such as the Faber-Jackson relation and the Fundamental Plane of spheroids (Hatton et al. 2003).

Readers who are familiar with the GalICS model will know that, in the code, gas is not moved directly from the disc to the bulge but it passes through a transitional component called the starburst. The star formation law has exactly the same form (Eq. 2) for all three components, but the starburst is assumed to have scale length that is equal to one tenth of the disc scale-length. Therefore, the starburst dynamical time that enters Eq. (2) is ten times shorter than the bulge dynamical time, which implies a factor of ten increase in the SFR. Stars formed in the starburst are moved to the bulge after they have reached an age of 100 Myr and the only gas in the bulge is that from stellar mass loss. However, it is not necessary to enter this level of detail to understand any of the conclusions of this article. We shall therefore simply speak of discs and bulges, where by bulge we mean the sum of the bulge and the starburst.

It follows from our discussion that while disc star formation is always stream fed, bulge star formation can be caused by two processes, since both gas-rich mergers and violent disc instabilities (such as those deriving from fast accretion of cold streams) contribute to bulge star formation. This point is important for the interpretation of our results and will be discussed further later on.

2.4 Feedback

We conclude our presentation of the GalICS model with a brief description of how it handles stellar evolution and feedback.

Stars are evolved between snapshots using substeps of at most 1 Myr. During each sub-step, stars release mass and energy into the interstellar medium. Most of the mass comes from the red giant and the asymptotic giant branches of stellar evolution, while most of the energy comes from shocks due to supernova explosions. The enriched material released in the late stages of stellar evolution is mixed with the cold phase, while the energy released from supernovae is used to reheat the cold gas and to return it to the hot phase in the halo (Eq. 5). Reheated gas is ejected from the halo if the potential is shallow enough. The rate of mass loss through supernova-driven winds \dot{M}_w is determined by the equation

$$\frac{1}{2} \dot{M}_w v_{\text{esc}}^2 = \epsilon_{\text{SN}} \eta_{\text{SN}} E_{\text{SN}} \dot{M}_{\text{star}}, \quad (5)$$

where $E_{\text{SN}} = 10^{51}$ erg is the energy of a supernova, $\eta_{\text{SN}} = 0.0093$ is the number of supernovae for $1 M_{\odot}$ of stars formed and v_{esc} is the escape velocity (Dekel & Silk 1986).

In GalICS, feedback is computed separately for each galaxy component. We use $v_{\text{esc}} \simeq 1.84 v_c$ for discs and $v_{\text{esc}} = 2\sigma$ for bulges/starbursts. The supernova efficiency $\epsilon_{\text{SN}} \simeq 0.2$ is similar to that commonly adopted in SAMs (Somerville & Primack 1999; Cole et al. 2000).

2.5 Quenching of star formation

As in Cattaneo et al. (2008), in haloes above M_{crit} , we do not just shut down gas accretion; we also shut down star formation. Moreover, we suppress gas accretion in galaxies where the bulge mass is larger than half the total stellar mass. As long as $M_{\text{halo}} < M_{\text{crit}}$, gas accretion can start again if this condition is no longer verified.

These further assumptions were introduced not based on a compelling physical argument, (though some physical justifications are possible; see below), but rather because we found that they improved the agreement with the observed galaxy colour - magnitude distribution, even though an acceptable fit could be obtained without them (Fig. 9 of Cattaneo et al. 2006 shows how these further assumptions improve the basic model in which we simply shut down gas accretion at $M_{\text{halo}} > M_{\text{crit}}$).

The second assumption implies that many ($> 57\%$) red-sequence galaxies are quenched following a merger event that has caused the bulge mass to increase above the disc mass (note that the bulge mass never exceeds the disc mass by violent instability alone; see previous discussion). This is particularly true for galaxies around $M_* \sim 10^{11} M_{\odot}$ (Cattaneo et al. 2008, Fig. 3).

Two possible physical explanations for this behaviour are i) quenching induced by quasar feedback following black hole growth activated by merging (Springel et al. 2005; Hopkins et al. 2006; also see Cattaneo et al. 2009 for a review), and ii) morphological quenching as proposed by Martig et al. (2009). These authors presented a picture in which a large bulge stabilizes disc instabilities and therefore inhibits the formation of spiral arms, which are the main sites of star formation in a spiral galaxy.

In the first case, star formation is quenched because the cold gas is blown out. In the second, the gas is not blown out, but it is prevented from making stars. One should notice, however, that shutting down gas accretion and shutting down star formation produce very similar effects when plugged into our semianalytic model.

3 BRIDGING PAST AND PRESENT

Having described the model, we are now ready to explain how we analyse the results. As this work is focussed on the nature of high- z SFGs and the progenitors of low- z red (early-type) galaxies, we need a procedure to assign $z = 0$ descendants to high- z galaxies and high- z progenitors to $z = 0$ galaxies. One way to do it is to follow the galaxy flow on a stellar mass - redshift diagram.

Fig. 1 has been constructed by separating the stellar mass - redshift diagram into tiles. For each tile, that is, for each a stellar mass and redshift interval, we take the galaxies one by one and ask what is the median mass of their immediate descendants. Once we have this information, we can use a trait to connect each tile to the tile in the following timestep that corresponds to the median descendant mass. This is what we have in the left panel of Fig. 1, which shows the ‘forward’ flow of galaxies on the $M_* - z$ diagram.

The middle panel is very similar, but it shows the ‘backward’ flow. Instead of looking for the median mass of the descendants of the galaxies on a tile, we look for the median

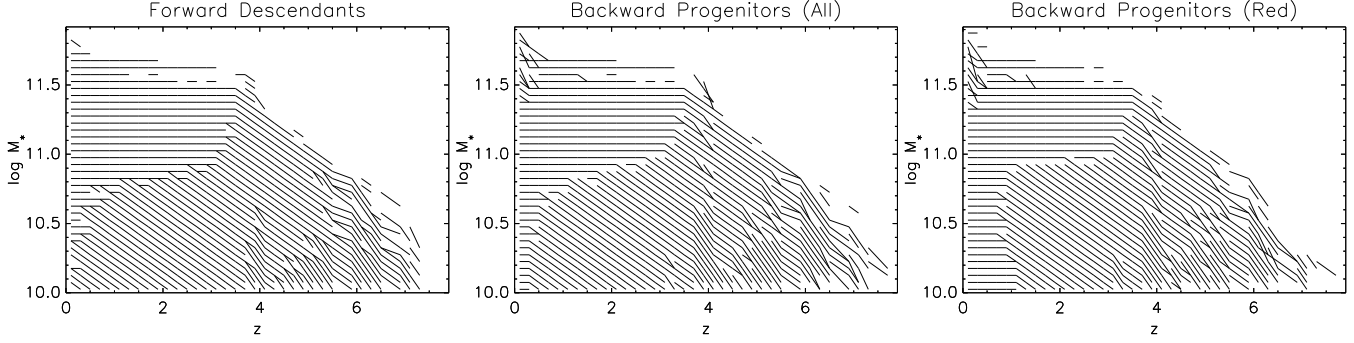


Figure 1. Forward (left panel) and backward (central and right panels) evolutionary tracks of galaxies on the M_* - z plane. The left panel and the central panel are for the entire population. The right panel is only for galaxies that are on the red sequence at $z = 0$. Forward evolutionary tracks are constructed by linking a tile with the tile corresponding to the median mass of the descendant galaxies. Backward evolutionary tracks are constructed by linking a tile with the tile corresponding to the median mass of the main progenitors.

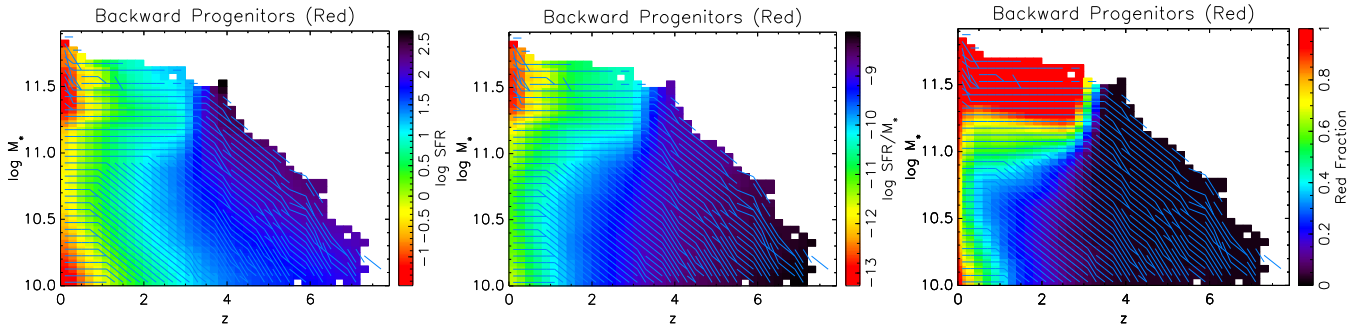


Figure 2. Median SFR (left panel), specific SFR (centre panel) and fraction of red galaxies (right panel) on each tile of the M_* - z diagram. The curves are the same backward evolutionary tracks as in the right panel of Fig. 1.

mass of their main progenitors. So we connect each tile with another tile at the previous timestep.

The right panel is identical to the middle panel, except that it only traces back in time the progenitors of those galaxies that are red at $z = 0$.

Let us start by comparing the left and middle panels. We see that the forward and the backward evolution are not identical. The reason for this difference is easily explained. It is possible that most of the galaxies in two mass bins, M_1 and M_2 , at redshift z_1 come from the same mass bin, M_3 , at the previous redshift step $z_2 > z_1$. That means that some of the galaxies in M_3 at z_2 end up in M_1 at z_1 and some in M_2 . Let us assume that most end up in M_1 . Then only M_1 at z_1 will be linked to M_3 at z_2 in the forward evolution but both M_1 and M_2 at z_1 will be linked to M_3 at z_2 in the backward evolution.

This is what happens, for instance, in the mass bin $M_* \sim 10^{11.5} - 10^{11.55} M_\odot$ at $z \sim 3.8 - 4$. The very few galaxies on this tile are galaxies that belonged to the mass bin $M_* \sim 10^{11.3} - 10^{11.35} M_\odot$ at the previous timestep and that have experienced a sudden mass increase of $\sim 60\%$ due to a major merger (Fig. 1, middle panel). However, most of the galaxies with $M_* \sim 10^{11.3} - 10^{11.35} M_\odot$ at $z \sim 4 - 4.2$ do not experience a merger at the next timestep (Fig. 1, left panel).

Let us now compare the middle panel (the progenitors of all galaxies) to the right panel (the progenitors of red galaxies). At high M_* , we hardly see any significant difference. This should not surprise us because, at $z = 0$, most

galaxies with $M_* > 10^{11} M_\odot$ are red. At $M_* < 10^{10.8} M_\odot$, we see that most red galaxies (right panel) have not grown in mass for the last half the cosmic lifetime (since $z \sim 1$). In contrast, the overall galaxy population (middle panel) is dominated by objects that are still growing or that have grown until very recently. The same difference is also seen when we compare the left panel and the middle panel.

While we have spent three paragraphs to clarify these differences, the main result that emerges from a comparison of the right and the left panel in Fig. 1 is, in fact, their similarity, particularly at high masses, which constitute the focus of this article. Hence, galaxy histories can be described as one-parameter family of curves, with the stellar mass at any given redshift as the key quantity that determines on which evolutionary tracks a galaxy lies. This is also the reason why we can establish a one-to-one relation between $z = 0$ galaxies and their high- z parent population, at least in a statistical sense¹.

¹ The assumption that galaxy star-formation and stellar masses form a one-parameter family has been cited before in other contexts. It is implicit, for example, in the star-forming main sequence of Noeske et al. (2007a) and Noeske et al. (2007b), in which galaxies of a given stellar mass today were fitted to a unique star-formation history. It is also implicit in the halo abundance matching model of Conroy & Wechsler (2009), in which they assumed that the star formation rate was uniquely determined by halo mass at each redshift. These and similar prescriptions tend to produce a one-parameter family of galaxies labeled by mass.

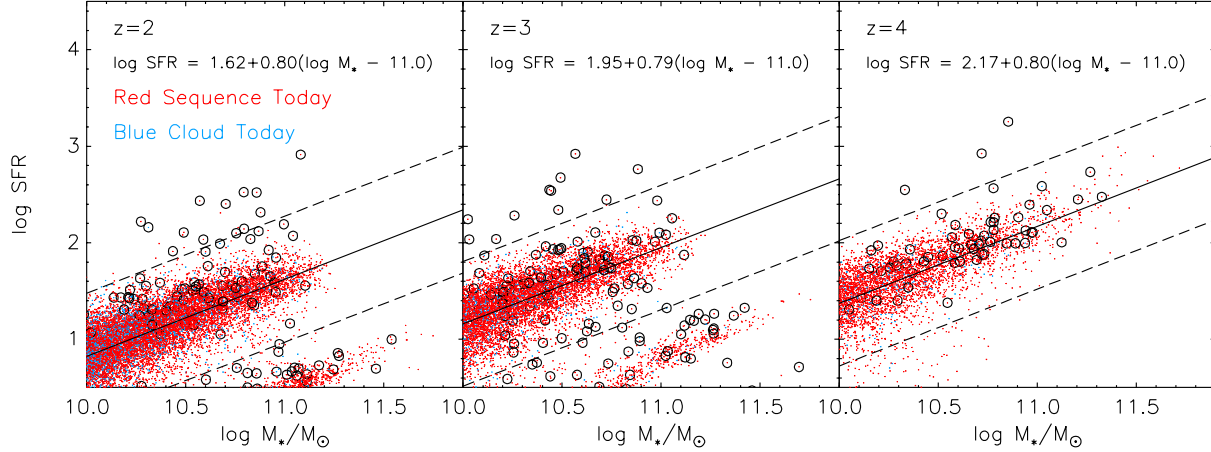


Figure 3. SFR vs. galaxy stellar mass for all model galaxies in the computational box at $z = 2$ (left), $z = 3$ (centre) and $z = 4$ (right). Each galaxy is shown with a red or a blue symbol depending whether its descendant at $z = 0$ lies on the red sequence or the blue cloud. Symbols surrounded by a black circle correspond to ongoing mergers with mass ratio greater than 1:4 (major mergers). The solid lines show, for each redshift, the best linear least-square fit to the main sequence of SFGs, while the dashed lines mark $\pm 3\sigma$.

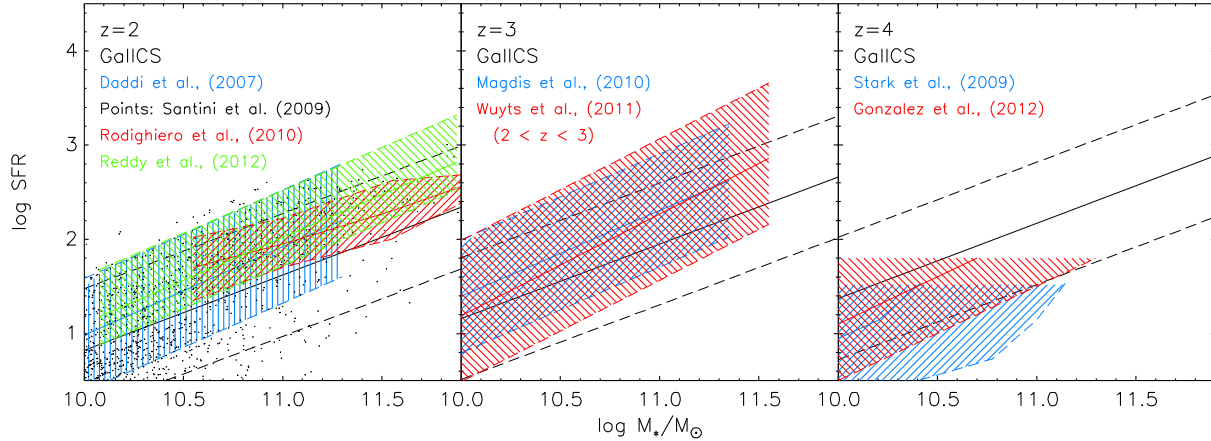


Figure 4. The model results shown in Fig. 3 are compared with the galaxies of Santini et al. (2009; $z = 2$) and different observational determinations of the SFR- M_* relation at $z = 2$ (Daddi et al. 2007; Rodighiero et al. 2010; Reddy et al. 2012), $z = 3$ (Magdis et al. 2010; Wuyts et al. 2011), and $z = 4$ (Stark et al. 2009; Gonzalez et al. 2012). The solid and dotted lines at $z = 2, 3, 4$ show the model relation and are the same as in Fig. 3. They have been added to facilitate the comparison with Fig. 3.

This kind of diagram is useful to study also the evolution in the star formation properties of the galaxy population. The tracks in Fig. 2 are the same backward evolutionary tracks that we already showed in the *right* panel of Fig. 1, but now we have added colour to display the median star formation rate (SFR; left panel), the median specific star formation rate (SSFR; middle panel), and the fraction of red galaxies (right panel) on each mosaic tile. It is important to keep in mind that the tracks on the three panels of Fig. 2 are all and only for galaxies that end up on the red sequence at $z = 0$. This is why, in the right panel of Fig. 2, the fraction of red galaxies at $z = 0$ is unity for all values of stellar mass.

Here a red galaxy is defined to be in the red sequence of the colour-mass diagram. We chose the division between the red sequence and blue cloud by eye as the criterion to separate red and blue galaxies at each timestep.

The left panel of Fig. 2 shows that, in our model, there is an almost one-to-one relation between the passive popula-

tion of $z \sim 0$ massive galaxies (the galaxies with the lowest SFRs ever) and the population of massive $z = 3 - 6$ galaxies with $\text{SFR} > 100 M_\odot \text{yr}^{-1}$ (which comprises the strongest starbursts in the Universe). While at low- z , the most massive galaxies are those with the lowest SFRs, at $z > 3$ the highest SFRs are predicted to be in the most massive galaxies at those redshifts.

The right panel of Fig. 2 shows that, in our model, the most massive galaxies grow along the blue sequence until $z \sim 3.5$, and that the red sequence begins to emerge at $z \sim 3 - 3.5$. After this point, most giant ellipticals evolve passively. One can see clearly from Fig. 2 that the point where the SFR drops and galaxies move to the red sequence is exactly where the curves $M_*(z)$ go horizontal. This is logical, since the stellar mass stops increasing when star formation shuts down. This shut down is a direct consequence of the assumption that gas accretion and star formation shut down above a critical mass $M_{\text{crit}}(z)$, which underpins all the results of Cattaneo et al. (2006), Cattaneo et al. (2008), and

this article. Restart of galaxy growth at $z \lesssim 0.5$ is due to dry mergers at the centres of groups and clusters. This effect is likely to be overestimated because our model does not include tidal stripping (discussion in Cattaneo et al. 2008).

The middle panel of Fig. 2 shows a trend, in which the typical SSFR decreases with time and lower at higher stellar masses.

4 HIGH-REDSHIFT STAR-FORMERS AND THEIR DESCENDANTS

Having described how we map the high- z galaxy population into the low- z one and vice versa, we are now ready to present our results. In this Section, we look at high- z ($z \sim 2-4$) SFGs and we follow their descendants at $z = 0$.

Fig. 3 shows the SFR - stellar mass relation at $z = 2, 3, 4$. Most galaxies (symbols) lie on a diagonal strip where the SFR grows with the stellar mass M_* . This strip is the main sequence of SFGs (Noeske et al. 2007b; Elbaz et al. 2011). Between $z = 4$ and $z = 3$, a second strip emerges parallel to the former, the tip of which is visible in the panel at $z = 3$. It is the sequence of passive galaxies. Galaxies on the latter have much lower SFR for a given stellar mass and this is where, already at $z = 3$, the most massive galaxies lie.

We define the SFG population as follows. We separate the main sequence of SFGs from the passive population with the line $\log \text{SFR} = \log M_* + c(z)$ where $c(z) = (-10, -9.7, -9.5)$ for $z = (2, 3, 4)$. We then perform a linear least squares fit to the galaxies that lie above this dividing line and that are more massive than $10^{10} M_\odot$. The fit is the solid line in Fig. 3. We compute the standard deviation σ of the points from the fit and consider the galaxies within 3σ of the fit to be the main sequence of SFGs (the galaxy population within the two dashed lines). We define an SFG to be any galaxy above the lower dashed line, including the outliers from the main sequence of SFGs. We, therefore, do not adopt an absolute SFR criterion to define SFGs, though we introduce a stellar-mass cut at $M_* > 10^{10} M_\odot$. One can see from Fig. 3 that, with this cut, our simulated-galaxy sample is ‘complete’ down to $\sim (100, 60, 30) M_\odot \text{ yr}^{-1}$ at $z = (4, 3, 2)$. In the next Section, we shall start from massive red galaxies at $z = 0$ and we shall track their progenitors back in time.

In our model, the normalisation of the SFR - M_* relation decreases from high to low z for both star-forming and passive galaxies. A least squares fit to the main sequence of SFGs, $\text{Log SFR}/(M_\odot \text{ yr}^{-1}) = a(\text{Log } M_*/M_\odot - 11) + b$ yields similar slope of $a \sim 0.80$ in each redshift bin, but the normalisation at $M_* = 10^{11} M_\odot$ decreases from $\text{SFR} \sim 160 M_\odot \text{ yr}^{-1}$ at $z = 4$ to $\text{SFR} \sim 100 M_\odot \text{ yr}^{-1}$ at $z = 3$ and $\text{SFR} \sim 40 M_\odot \text{ yr}^{-1}$ at $z = 2$. Hence, the number of galaxies above a given SFR decreases with time. For instance, the number density of galaxies with $\text{SFR} > 100 M_\odot \text{ yr}^{-1}$ is predicted to decrease from ~ 170 per $(150 \text{ Mpc})^3$ at $z = 4$ to ~ 50 and ~ 7 per $(150 \text{ Mpc})^3$ at $z = 3$ and $z = 2$, respectively.

Fig. 4 compares the model results of Fig. 3 with observational determinations of the SFR - M_* relation. Daddi et al. (2007; $z = 2$), Santini et al. (2009; $z = 2$), Rodighiero et al. (2010; $z = 2$), Reddy et al. (2012; $z = 2$), Stark et

al. (2009; $z = 4$), and Gonzalez et al. (2012; $z = 4$) used the Salpeter IMF in their estimates of M_* , while Magdis et al. (2010; $z = 3$) and Wuyts et al. (2011; $z = 3$) used the Chabrier IMF. We have scaled their values to be consistent with the Kennicutt IMF used in Cattaneo et al. (2006) and Cattaneo et al. (2008). To pass from the Salpeter IMF and the Chabrier IMF to the Kennicutt IMF, we have used the relations found in Bell et al. (2003); Fardal et al. (2007); Treyer et al. (2007).

The slope and the scatter of the model relations at $z = 2$ and $z = 3$ are quite similar to those that we find in the data. However, the normalisation of the SFR - M_* relation at $M_* = 10^{11} M_\odot$ that we find in our model at $z = 2$ is $\sim 2-3$ times lower than that found in observational studies (Daddi et al. 2007; Santini et al. 2009; Rodighiero et al. 2010; Reddy et al. 2012). We find the same discrepancy at $z = 3$, when we compare our results to the observational determinations by Magdis et al. (2010) and Wuyts et al. (2011).

At $z = 4$ our SFR - M_* relation appears to be higher than the observational determinations by Stark et al. (2009) and Gonzalez et al. (2012). However, the comparison with the data at $z = 4$ requires extreme caution for two reasons. First, the blue and the red hatched areas finish abruptly at $\sim 10^{1.5} M_\odot/\text{yr}$ and $\sim 10^{1.8} M_\odot/\text{yr}$, respectively, because the relation at $z = 4$ is given in bins of SFR, rather than in bins of M_* . Secondly, the data by Stark et al. (2009) are not dust corrected.

Globally, the model is not doing too bad considering that the rough agreement in Fig. 4 has been obtained without tuning any free parameter. We have simply taken a model that is already published (Cattaneo et al. 2006, 2008) and that works well at $z = 0$, and we have analysed its predictions for the SFR - M_* relation at $z = 2-4$. Admittedly we have also required that this model reproduces the luminosity function of Lyman-break galaxies at 1700 angstrom restframe. However, this is no guarantee to reproduce the SFR - M_* relation, particularly since many SFR measurements come from infrared data.

In closer detail, the discrepancy with the observed SFR - M_* relation at $z = 2$ was not unexpected because we know that the cosmic SFR density predicted by our model at $z = 2$ is at the lower limit of the range allowed by observations (Fig. 8 of Cattaneo et al. 2006), and that all semianalytic models underpredict sub-mm counts, unless they invoke a top-heavy stellar initial mass function (Baugh et al. 2005; Lacey et al. 2008).

We should also note, however, that at $z = 1$, where there are more data, Noeske et al. (2007b) and Chen et al. (2009) find a substantially lower normalisation of the SFR - M_* relation than Elbaz et al. (2007) and Santini et al. do (Elbaz et al. 2007 and Daddi et al. 2007 are the same group).

Having discussed the comparison with the data, we now take a closer look at the results of our model.

Fig. 3 shows that, at $z = 4$, a lot of the SFGs with $\text{SFR} > 100 M_\odot \text{ yr}^{-1}$ are objects at the massive end of the SFR sequence. In contrast, at $z = 2$, SFGs with $\text{SFR} > 100 M_\odot \text{ yr}^{-1}$ are outliers from the main sequence.

The main sequence of SFGs represents the normal SFG population at a given redshift. Yet, at $z \sim 4$, the tip of the main sequence of SFGs reaches SFRs of about $1000 M_\odot \text{ yr}^{-1}$.

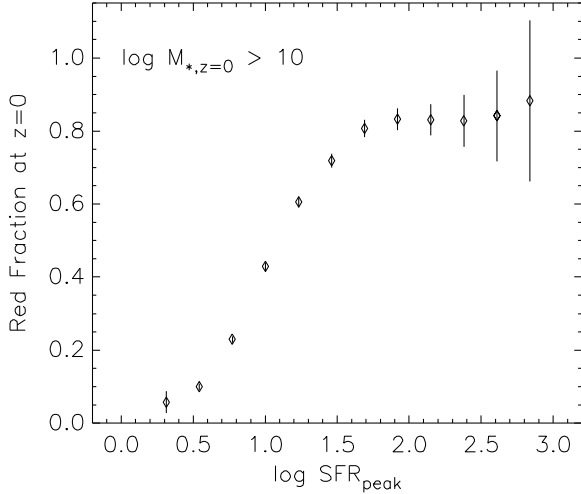


Figure 5. Fraction of galaxies on the red sequence at $z = 0$ as a function of peak star formation rate. The error bars are Poissonian errors. This figure includes all galaxies with $M_* > 10^{10} M_\odot$ at $z = 0$.

Some galaxies have very high SFRs (up to thousands of Solar masses per year) that cause them to be outliers from the main sequence of SFGs. It is apparent from Fig. 3 that these galaxies are almost always mergers, because objects which have experienced a greater than 1:4 merger in the last 300 Myr have been surrounded with a black circle.

Fig. 3 suggests that mergers are necessary to explain the highest SFRs at any given z , but that they do not drive the bulk of star formation at high redshift, most of which occurs along the main sequence of SFGs. The circled symbols account for 0.6, 1.2, and 1.4% of the objects on the main sequence of SFGs (i.e., those between the 3σ lines in Fig. 3) at $z = 2, 3, 4$, respectively. The percentages increase to 54, 92, and 100% if we look at outliers above the main sequence of SFGs, defined as galaxies that lie more than 3σ above the fit to the main sequence of SFGs (upper line in Fig. 3).

Galaxies have been plotted in red or blue depending on whether their descendants lie on the red sequence or the blue cloud of the colour - M_* diagram at $z = 0$. The criterion used to separate red and blue galaxies is $U - B > 0.95 + 0.06(\log M_*/M_\odot - 10.0)$.

A strong result that emerges from Fig. 3 is that virtually all massive SFG galaxies evolve into the red sequence at $z = 0$. The fraction of SFGs that end up on the red sequence depends slightly on mass, SFR and redshift. We find that $\sim 95 - 98\%$ of high- z SFGs with $M_* > 10^{11} M_\odot$ evolve into red-sequence galaxies by $z = 0$ (these values correspond to $z = 2$ and $z = 4$, respectively). At lower masses ($10^{10} M_\odot < M_* < 10^{11} M_\odot$), the fraction of SFGs that end up of the red sequence is lower and exhibits a slightly stronger dependence on redshift. The SFGs with $10^{10} M_\odot < M_* < 10^{11} M_\odot$ that evolve into red-sequence galaxies by $z = 0$ are 86%, 91%, and 97% at $z = 2, 3, 4$, respectively.

Above a given SFR, say $100 M_\odot \text{ yr}^{-1}$, objects have a substantial probability of ending up on the red sequence at $z = 0$ (96%, 95% and 97% for objects with $\text{SFR} > 100 M_\odot \text{ yr}^{-1}$ at $z = 2, 3, 4$, respectively).

Fig. 5 shows the probability that a $z = 0$ galaxy is on the red sequence as a function of its peak SFR. It shows

that 80% of all objects that have ever reached $> 40 M_\odot \text{ yr}^{-1}$ evolve into red-sequence galaxies.

We do not argue that the peak SFR of a galaxy is the most important factor in determining if it ends up on the red sequence or the blue cloud. But since the SFR of a galaxy at any time put a lower limit to its peak SFR, Fig. 4 is useful because, given a SFR measurement, it gives the minimum probability that an observed galaxy has to end up on the red sequence at $z = 0$.

In fact, we do not argue at all that absolute SFR provides a physical criterion to tell if a galaxy becomes quenched. Galaxy mass (due to its link to halo mass) and morphology are, in this sense, much more relevant. The purpose of this analysis is rather to show the correlation between one of the most basic properties that one can measure in a high- z galaxy (SFR) and what our model predicts for its later evolution.

5 THE PROGENITORS OF MASSIVE RED GALAXIES

In Section 3, we have looked at high-redshift ($z \sim 2 - 4$) SFGs with $M_* > 10^{10} M_\odot$ and we have found that most of them evolve into massive red-sequence galaxies by $z = 0$. We now do the opposite. We start from massive red-sequence galaxies in the local Universe and we reconstruct their SFR histories by tracking their most massive progenitor back in time.

Fig. 6 has been constructed by selecting eight galaxies with $M_* \gtrsim 10^{11.5} M_\odot$ today. These galaxies have been chosen to illustrate the variety of star formation histories of today's massive red galaxies. The total SFR as a function of z (black solid line) has been decomposed into the contributions of disc and bulge. Mergers with mass ratios greater than 1:4 (major mergers) are highlighted with an asterisk symbol. The vertical dashed lines show the redshifts at which the dark matter haloes of these galaxies have passed M_{crit} .

In galaxies (a), (b) and (c), disc star formation dominates the total SFR before star formation is quenched at $3 < z < 4$ (the fact that the bulge SFR is higher than the disc SFR after quenching is an artifact due to assuming a gas-surface-density threshold for disc star formation but not for bulge star formation). In galaxy (d), the two are comparable just before star formation is quenched. Galaxy (c) experienced no major mergers (in Fig. 6, major mergers are marked with asterisks). Galaxies (a), (b) and (d) experienced one major merger each at $z < 1$, long after they ceased to make stars. In conclusion, the mergers experienced by galaxies (a), (b), (c) and (d) are dissipationless and the bulge star formation in galaxies (a), (b), (c) and (d) is driven not by mergers but rather by disc instabilities.

Galaxies (e), (f), (g) and (h) had 2-3 major mergers each and they exhibit strong SFR peaks at the time of their first merger, which occurs before quenching, when the galaxies were still gas-rich. There is a clear direct link between dissipative mergers and strong starbursts in the bulge component, which cause it to dominate the SFR temporarily. In galaxies (e) and (f), mergers cause the SFR to increase by a factor of ~ 4 . In galaxy (h), the SFR increases by a factor of ~ 10 . It is also interesting to note that while galaxies (e), (f) and (g) go back to normal ‘quiescent’ star formation after a

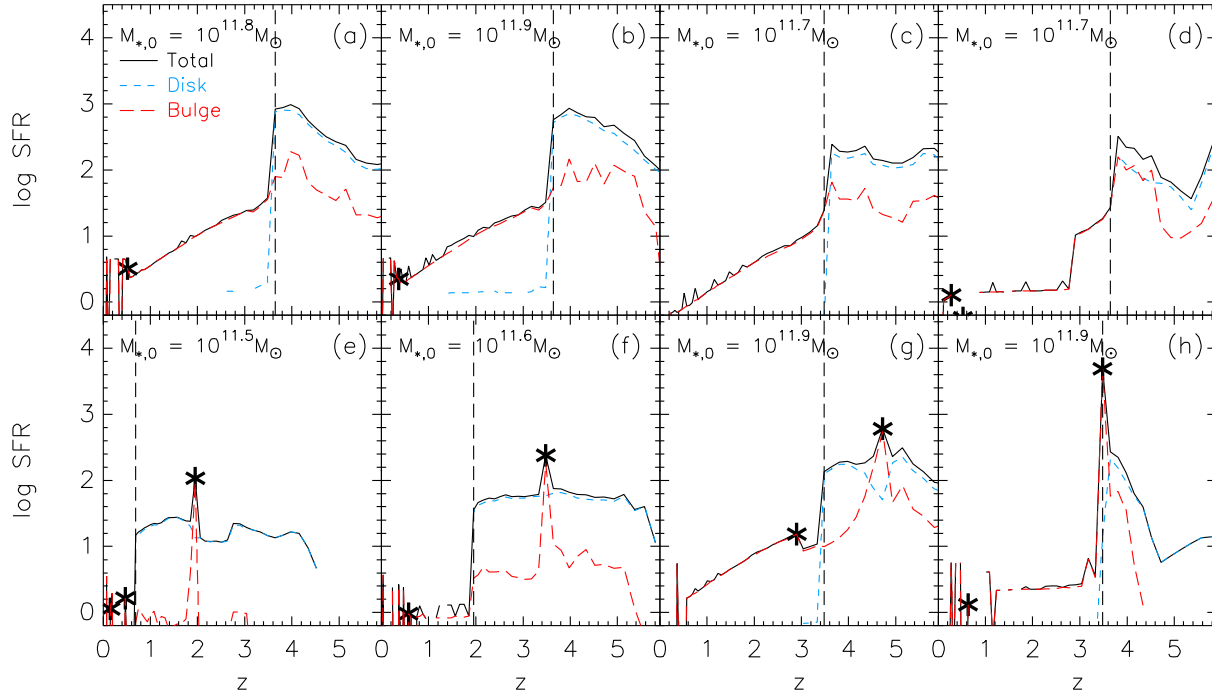


Figure 6. The SFR histories of eight red-sequence galaxies selected for illustrative purposes. Each SFR history has been decomposed into disc (blue) and bulge (red) star formation. The stellar mass of each galaxy at $z = 0$ has been shown in the corresponding panel. Major mergers (with ratio $> 1 : 4$) have been marked with asterisks. Most of them are ‘dry’ (dissipationless) mergers occurring after the galaxies have ceased to make stars. ‘Wet’ (gas-rich) mergers are accompanied by strong starbursts, characterised by a sharp rise and a fall in the bulge SFR. The fact that the bulge SFR declines continuously and is higher than the disc SFR after quenching is an artifact due to assuming a gas-surface-density threshold for disc star formation but not for bulge star formation, which, after shutdown, is fed by stellar mass loss only.

merger-driven starburst - if one can call quiescent a galaxy like (g) with a disc SFR $> 100 M_{\odot} \text{ yr}^{-1}$, - in galaxy (h) the merger-driven starburst coincides with the shutdown of star formation.

Merger-driven starbursts are, by construction, short-lived. We have verified that in galaxies (e), (f) and (g) only a small fraction of the final galaxy stellar mass was formed in the bulge even if the highest SFR occurred in the bulge. Galaxy (h) is the prototypical example of an elliptical galaxy that makes most of its stars in a single merger-driven burst at high z . However, objects of this type are exceedingly rare. They can be counted on the fingers of one hand in our computational volume of $(150 \text{ Mpc})^3$.

With insight from these particular cases, we are now ready to look at the statistical properties of the progenitors of red-sequence galaxies. We split the latter into three ranges of stellar mass at $z = 0$ (lower intermediate mass: $10^{10.5} M_{\odot} < M_* < 10^{11} M_{\odot}$; upper intermediate mass: $10^{11} M_{\odot} < M_* < 10^{11.5} M_{\odot}$; high mass: $M_* > 10^{11.5} M_{\odot}$) and characterize the SFR histories of the disc and the bulge of each galaxy in terms of two properties: the peak SFR and the redshift at which the SFR reaches its peak value.

Fig. 7 shows the joint distribution of SFR_{peak} and z_{peak} for galaxies in which the peak SFR is linked to star formation in the bulge component (above) and to the disc component (below). The histograms in Figs. 8-9 show the distributions for SFR_{peak} and z_{peak} separately. In these figures, blue histograms are those galaxies whose peak SFR was in the disc (they correspond to the lower panels of Fig. 7), while

red histograms are those whose peak SFR was in the bulge (they correspond to the upper panels of Fig. 7).

Figs. 7-9 show that the typical peak SFR is tens of Solar masses per year for lower intermediate-mass red galaxies, about a hundred Solar masses per year for upper intermediate-mass red galaxies and several hundreds Solar masses per year for high-mass galaxies, but this is only a statistical statement. Even among lower intermediate-mass galaxies, there are objects with $\text{SFR}_{\text{peak}} \sim 1000 M_{\odot} \text{ yr}^{-1}$. In all ranges of mass, galaxies in which the peak SFR occurs *in the disc* are much more numerous than galaxies in which the peak SFR occurs in the bulge. To put it quantitatively, only 11%, 12%, and 16% of the red-sequence galaxies in the stellar mass intervals $10^{10.5} M_{\odot} < M_* < 10^{11} M_{\odot}$, $10^{11} M_{\odot} < M_* < 10^{11.5} M_{\odot}$, and $10^{11.5} M_{\odot} < M_* < 10^{12} M_{\odot}$ have experienced a SFR peak dominated by bulge star formation.

As we argued at the end of Section 2.3, disc star formation is always stream-fed in the sense that, by construction, discs can acquire gas from smooth accretion only. In contrast, both mergers and rapid smooth gas accretion contribute to bulge star formation. Major mergers do it directly, by bringing gas into the starburst/bulge component. Gas accretion and minor mergers do it indirectly, by causing a sudden increase in the gas content of the disc, which becomes unstable and transfers mass to the bulge. Thus the counts in the upper panel of Fig. 7 and the red histograms in Figs. 8-9 represent *upper limits* to merger-driven SFR, and we refer to these histograms loosely as the merger-driven contribution.

Therefore, our model makes two strong predictions. The

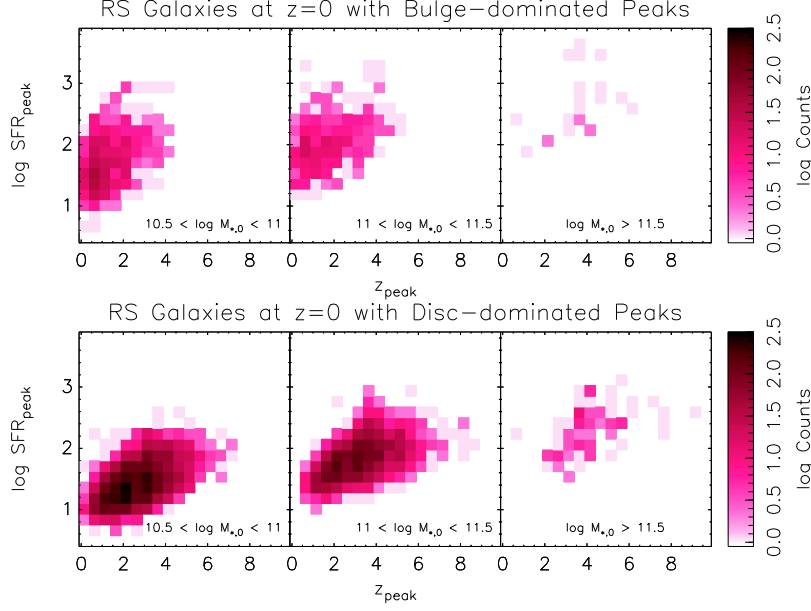


Figure 7. The joint distribution of peak SFR and redshift of peak SFR for $z = 0$ red-sequence galaxies in three bins of $z = 0$ stellar mass: $10^{10.5} M_{\odot} < M_{*} < 10^{11} M_{\odot}$, $10^{11} M_{\odot} < M_{*} < 10^{11.5} M_{\odot}$, and $M_{*} > 10^{11.5} M_{\odot}$. The upper and lower panels show the $\text{SFR}_{\text{peak}} - z_{\text{peak}}$ distribution for galaxies with $\text{SFR}_{z=z_{\text{peak}}}^{\text{bulge}} > \text{SFR}_{z=z_{\text{peak}}}^{\text{disc}}$ and $\text{SFR}_{z=z_{\text{peak}}}^{\text{bulge}} < \text{SFR}_{z=z_{\text{peak}}}^{\text{disc}}$, respectively.

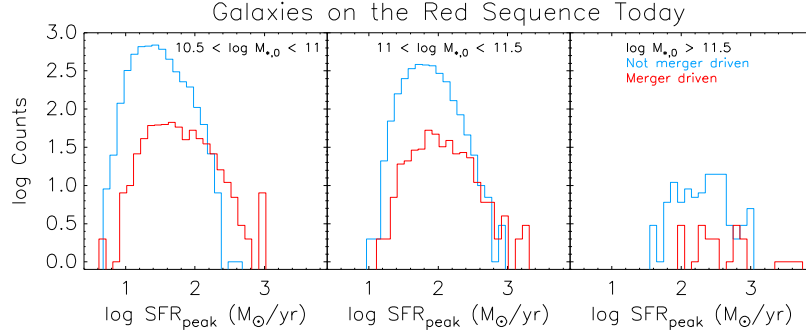


Figure 8. Distribution for the value of the peak SFR for red-sequence galaxies in three intervals of stellar mass at $z = 0$: $10^{10.5} M_{\odot} < M_{*} < 10^{11} M_{\odot}$ (left), $10^{11} M_{\odot} < M_{*} < 10^{11.5} M_{\odot}$ (centre) and $10^{11.5} M_{\odot} < M_{*} < 10^{12} M_{\odot}$ (right). The distribution of SFR_{peak} has been shown separately for disc-dominated peaks (blue histograms) and bulge-dominated peaks (red histograms).

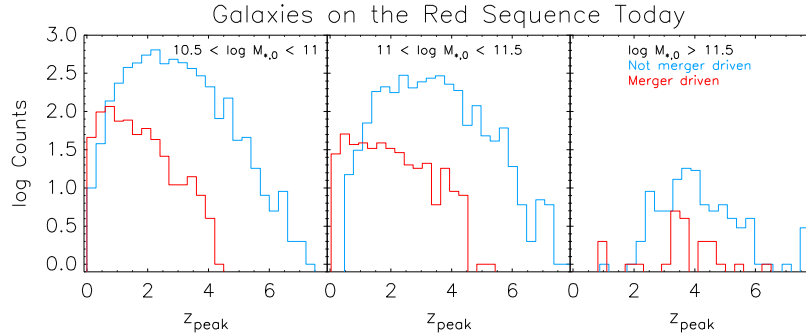


Figure 9. Distribution for the value of the redshift z_{peak} at which the SFR reaches its maximum for red-sequence galaxies in three intervals of stellar mass at $z = 0$: $10^{10.5} M_{\odot} < M_{*} < 10^{11} M_{\odot}$ (left), $10^{11} M_{\odot} < M_{*} < 10^{11.5} M_{\odot}$ (centre) and $10^{11.5} M_{\odot} < M_{*} < 10^{12} M_{\odot}$ (right). The distribution of z_{peak} has been shown separately for disc-dominated peaks (blue histograms) and bulge-dominated peaks (red histograms).

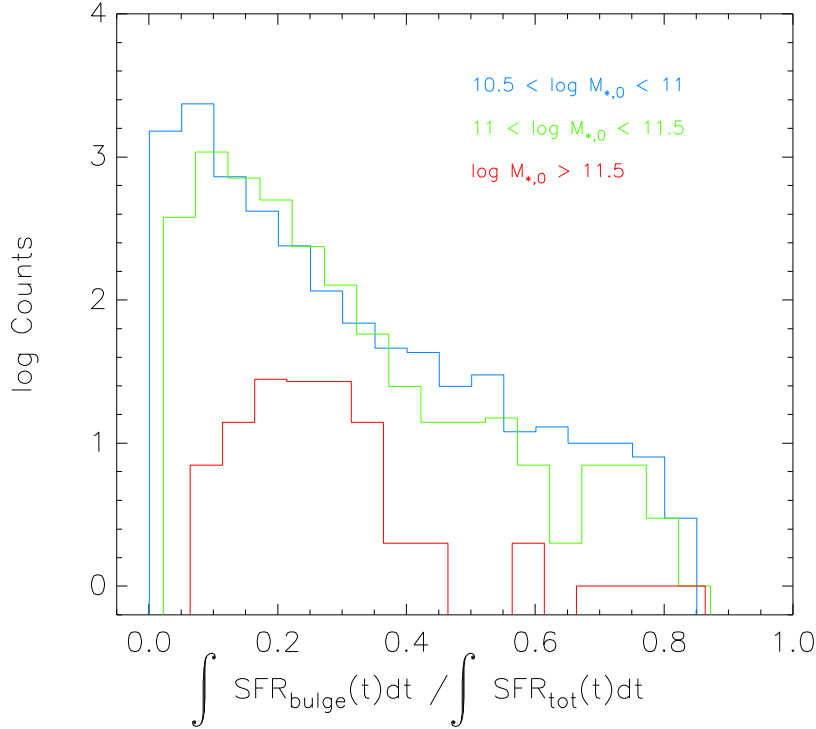


Figure 10. The contribution of bulge star formation to the total in situ star formation of red sequence galaxies (computed by following the galaxies’ main progenitors). The distribution of values for $\int_0^{t_0} \text{SFR}_{\text{bulge}}(t) dt / \int_0^{t_0} \text{SFR}_{\text{tot}}(t) dt$ is shown for three bins of stellar mass at $z = 0$: $10^{10.5} M_\odot < M_* < 10^{11} M_\odot$, $10^{11} M_\odot < M_* < 10^{11.5} M_\odot$, and $M_* > 10^{11.5} M_\odot$.

first is that, in most red galaxies, star formation was stream-fed, not merger-driven. The second is that, conversely, mergers are responsible for the most intense episodes of star formation at each redshift see Fig. 8, in agreement with data over a broad range of redshifts from $z \sim 0$ to $z \sim 2$.

The first conclusion can also be verified directly by taking the total SFR history and the bulge SFR history of each galaxy, computed by tracking the main progenitor back in time (i.e. the equivalent of the black and the red curves in Fig. 6), and by integrating them over time, to determine what fraction of the star formation that has occurred has been bulge star formation. Fig. 10 shows the distribution of values for $\int_0^{t_0} \text{SFR}_{\text{bulge}}(t) dt / \int_0^{t_0} \text{SFR}_{\text{tot}}(t) dt$ in the three bins of galaxy stellar mass $10^{10.5} M_\odot < M_* < 10^{11} M_\odot$, $10^{11} M_\odot < M_* < 10^{11.5} M_\odot$, $M_* > 10^{11.5} M_\odot$ (stellar masses at $z = 0$; t_0 is the current age of the Universe; and this figure is only for red-sequence galaxies). The average contribution of merger driven star formation for the three stellar mass bins is 11%, 15%, and 26%, respectively. Galaxies that formed most of their stars in merger-driven starbursts are rare, though it is quite usual that a quarter of the in-situ star formation in a massive early-type galaxy occurs via this mode. Most of the stars in a giant elliptical were not formed in situ, i.e. they were formed in smaller objects that merged with the galaxy, so we do not include either in the $\sim 1/4$ of bulge star formation or the $\sim 3/4$ of disc star formation.

Fig. 9 shows the distribution for the redshift z_{peak} at which the peak SFR occurs for the three ranges of masses. For lower intermediate-mass red galaxies, $z_{\text{peak}} \sim 2$. For

upper intermediate-mass red galaxies, $z_{\text{peak}} \sim 2.5 - 3.5$. For high-mass red galaxies, $z_{\text{peak}} \sim 4$.

The decrease of z_{peak} at lower masses is an aspect of downsizing. In our model, downsizing occurs because haloes with a lower mass at fixed z cross M_{crit} at a lower redshift (Fig. 4 of Cattaneo et al. 2008). In the same way M_{crit} is constant at $z \lesssim 3$ and increases at higher z , this also applies to the characteristic stellar mass M_*^{crit} with which galaxies enter the red sequence. The characteristic star formation rate of a galaxy that enters the red sequence at cosmic time t is $\text{SFR} \sim M_{\text{crit}}(t)/t$, which must decrease with t , since $\sim M_{\text{crit}}(t)$ is a non-growing function of t .

In Cattaneo et al. (2008), we analysed the time of peak SFR as a function of the final stellar mass for massive red-sequence galaxies. The results were found to be in agreement with that Thomas et al. (2005) inferred from the spectra of local early-type galaxies (Figs. 7-8 of Cattaneo et al. 2008).

Stream-fed star formation is responsible for most of the SFR peaks at all redshifts except perhaps at low-redshift ($z < 1$). In the stellar mass bins $10^{10.5} M_\odot < M_* < 10^{11} M_\odot$, $10^{11} M_\odot < M_* < 10^{11.5} M_\odot$, and $10^{11.5} M_\odot < M_* < 10^{12} M_\odot$, the red galaxies with $z_{\text{peak}} < 1$ are 9%, 5%, and 2%, respectively. If we look at this specific population, then the percentages of galaxies with merger-driven SFR peaks rise to 56%, 80% and 67% (instead of 11%, 12%, and 16%, as we saw before). These values would have been even higher if we took $z < 0.5$ instead of $z < 1$ (we would have found 81%, 98% and 100%, respectively). Fig. 7 tells us that these merger-driven peaks are typically about $50 M_\odot \text{yr}^{-1}$ for the lower-intermediate mass bin, and about $100 M_\odot \text{yr}^{-1}$ for the upper intermediate mass bin. Merger-driven star

formation is therefore relevant to those $M_* \sim 10^{11} M_\odot$ ellipticals that have formed via low-redshift gas-rich mergers such as those that we witness in local ULIRGs (see Cattaneo et al. 2011 for a discussion of the role of gas-rich mergers in the build-up of the galaxy population). The same trend is also seen in massive red-sequence galaxies: the SFR peak is usually stream-fed and is usually at $z \sim 4$ but in the few objects with merger-driven SFR peaks, the SFR peak is normally around $z \sim 3$. Most of the merger activity of massive red galaxies is predicted to be dissipationless and to occur at fairly low redshifts (Cattaneo et al. 2008; De Lucia & Blaizot 2007).

6 DISCUSSION AND CONCLUSION

To summarize, we find that: i) most galaxies that have experienced SFRs $> 40 M_\odot \text{ yr}^{-1}$ evolve into red-sequence galaxies, ii) 80% of the red-sequence galaxies with $M_* > 10^{11} M_\odot$ passed through a phase of high SFR ($\text{SFR}_{\text{peak}} > 40 M_\odot \text{ yr}^{-1}$) at $z > 1$, and iii) in $\gtrsim 90\%$ of these cases, this phase was stream-fed (merger ratio at peak SFR less than 1:4).

Still, mergers are necessary to explain the galaxies with the highest SFRs (e.g., the rare objects with SFRs of thousands of Solar masses per year). Furthermore, if we concentrate on $z = 0$ red-sequence galaxies with peak SFR at $z < 1$ (9%, 5%, and 2% of the objects in the three mass intervals), then the percentages of merger-driven SFR peaks rise to 56%, 80% and 67%, respectively. These values would have been even higher if we took $z < 0.5$ instead of $z < 1$. Hence, mergers are important for that small percentage of latter-day ellipticals that form in local ULIRGs, even though this cannot be the path via which most ellipticals formed (Ostriker 1980).

These figures (and all the others in this article) should be taken with caution because our model contains many arbitrary assumptions. Their uncertainties cannot be easily quantified but we believe they are probably greater than 10%. The purpose of the percentages quoted in this article is to illustrate the magnitude of the discussed phenomena. A change from 56% to 67% in the fraction of merger-driven peaks from one mass bin to another is not significant when one considers the uncertainties of the model. However, we prefer to give the exact numbers returned by our model accompanied by this disclaimer than to use vague language, where any quantitative information is lost.

The accuracy of a semianalytic model is established *a posteriori* by how well it reproduces the observations. Our model is in very good agreement with local data. The main problem is the discrepancy with the normalisation of the SFR - M_* relation at $z = 2 - 3$, which we have discussed in Section 4.

At $M_* = 10^{11} M_\odot$, our model predicts SFRs that are $\sim 2 - 3$ times lower than those inferred observationally by Daddi et al. (2007), Santini et al. (2009), Rodighiero et al. (2010), Magdis et al. (2010), Wuyts et al. (2011), Reddy et al. (2012), and, at the massive end of the main sequence of SFGs, by Huang et al. (2009). Our average SFR at a given stellar mass would still be too low compared to these data even if all the accreted gas were immediately converted into stars. The same basic problem is

found in the Munich model (e.g. Kitzbichler & White 2007) and in the Durham model, which proposes a top-heavy stellar initial mass function (IMF) as a possible solution (e.g. Baugh et al. 2005; Lacey et al. 2008).

Since Noeske et al. (2007a) and Chen et al. (2009) find a lower normalisation at $z = 1$ than the authors mentioned above, it is possible that these authors' SFR measurements at $z = 2$ need to be lowered, too, or that their masses are systematically underestimated. However, we also know that semianalytic models underpredict sub-mm counts, unless they invoke a top-heavy IMF. So either a top-heavy IMF is the solution, in which case there may be nothing wrong with our predicted SFRs, and it is the observationally derived SFRs that need to be corrected accordingly, or this signals a problem in our galaxy formation model. For instance, it is possible that our specific SFRs at $z = 4$ are too high (Fig. 4) because gas accreted at $z \gtrsim 4$ is converted into stars too rapidly (see, e.g., Krumholz & Dekel 2012), and this may be the reason why, in the model, there is not enough star formation at later epochs ($z \sim 2 - 3$; Fig. 3), though it also possible that $z = 4$ SFRs inferred by Stark et al. (2009) are underestimated due to dust.

In fact, one should also remember that the observational determinations of the SFR- M_* relation are themselves model-dependent. Measured SFRs and stellar masses depend on stellar-population synthesis models, dust models, and assumptions about the galaxies' SFR histories.

The question here is: to what extent these open issues affect our confidence in our results?

Could the underpredicted SFRs for a given M_* be due to an underestimate of the importance of mergers? Could our conclusion that the bulk of star formation in the ancestors of red galaxies is stream-fed be a result of our model somehow overestimating the importance of the stream-fed mode?

It is not inconceivable that our model may somehow underestimate the merger rate at high redshift, even though the assumptions that it makes are quite standard. The problem is that the entire main sequence of SFGs is shifted with respect to the data at $z = 2$. Mergers can temporarily increase the SFR by accelerating the conversion of gas into stars but they cannot change the average SFR for a given galaxy mass because a shorter star formation timescale means that at the end less fuel for star formation is left.

Let us now consider the second possibility, i.e. that the importance of stream-fed star formation is overestimated. Even though our model incorporates disc instabilities, in this article we have effectively identified stream-fed star formation with disc star formation and merger-driven star formation with bulge star formation. In reality, while disc star formation is always stream-fed, bulge star formation is partly merger-driven and partly stream-fed. By equating stream-fed star formation with disc star formation and merger-driven star formation with bulge star formation, we should underestimate the former and overestimate the latter, not the opposite, but let us analyse this point in closer detail.

Our semianalytic model has been run using the disc stability criterion (4) for a disc instability threshold parameter of $\eta = 0.7$. In other words, we assume that, within the disc half-mass radius, the steady state is that the mass in the disc is half the total mass. Dekel et al. (2009) have

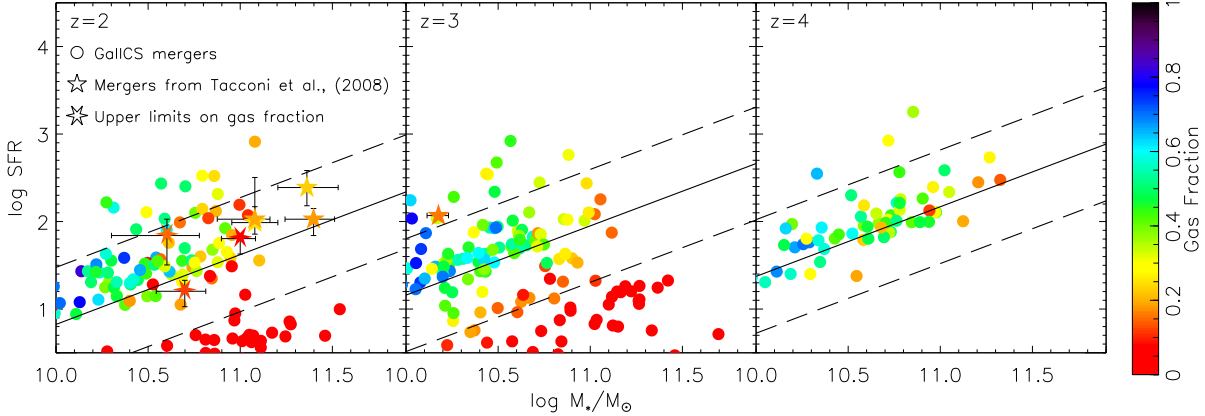


Figure 11. The gas content of major mergers at $z = 2, 3, 4$. GalICS galaxies that have experienced a merger in the last 300 Myr are shown as circles on the SFR- M_* diagram. Mergers observed in Tacconi et al., (2008) are marked as stars (six-point stars correspond to upper limits on the gas fraction). Their stellar masses and SFRs have been adjusted to the Kennicutt IMF. Each symbol is colour-coded according to the merger gas content, i.e., $M_{\text{gas}}/(M_* + M_{\text{gas}})$. jwbA circled star symbol indicates that the gas fraction is an upper limit, while the rest of the data from Tacconi et al. have uncertainties of about 0.08 in the fraction. The lines show the position of the main sequence of SF galaxies. They are the same as in Figs. 3 and 4.

explored a model for the instability of clumpy discs and they have been able to relate the disc-to-total mass ratio δ within the disc half-mass radius to σ/v_{rot} , the ratio of the velocity dispersion σ within the disc to the disc's rotation speed v_{rot} (also see Genel et al. 2012). For a Toomre disc instability parameter Q (Toomre 1964; Binney & Tremaine 2008, Chapter 6) of $Q \sim 1$ and a flat rotation curve, their model gives $\delta \sim \sqrt{2} \cdot \sigma/v_{\text{rot}}$. So, $\eta = 0.7$ is equivalent to $\sigma/v_{\text{rot}} \simeq 0.35$. In fact, spectroscopic observations of gas kinematics in massive discs at $z \sim 2$ give values closer to $\sigma/v_{\text{rot}} \simeq 0.2$ (Erb et al. 2004; Förster Schreiber et al. 2006; Cresci et al. 2009), which imply $\delta \sim 0.3$. Based on this analysis, the actual inflow due to disk instability in high- z clumpy discs is stronger than what GalICS assumes.

Still, our predicted bulge-to-total stellar mass ratios for blue galaxies are systematically on the high side at all masses (GalICS predicts a typical bulge-to-total mass ratio of $M_{\text{bulge}}/M_{\text{gal}} \sim 0.3$ for a blue galaxy with $M_r \sim -20.5$; Cattaneo et al. 2006, Fig. 10). Simply lowering the value of η would bring predicted bulge-to-total stellar mass ratios to values that are incompatible with the prevalence of late-type morphologies in the local galaxy population. This is why hydrodynamic simulations have for a long time experienced major difficulty in forming spirals with acceptable bulge-to-total stellar mass ratios, though they follow gas and stellar dynamics more self-consistently than semianalytic models do. Recent progress in forming spirals with acceptable bulge-to-total stellar mass ratios is linked to strong feedback that preferentially ejects gas from the central starburst (Governato et al. 2010; Guedes et al. 2011; Piontek & Steinmetz 2011; Brown et al. 2007; McCarthy et al. 2012). Therefore, a more physical description of disc instability must be accompanied by a more physical description of stellar feedback.

Based on this discussion, GalICS likely underestimates both the inflow into the bulge due to disc instability and the outflow from the bulge due to stellar feedback. So, part of the stream-fed star formation that we predict to occur in the disc may have occurred in the bulge, or vice versa (as

it is more likely, at least for spiral galaxies, whose bulge-to-stellar mass ratio are overpredicted). However, that does not change the relative importance of stream-fed and merger-driven star formation.

One may also worry that our SFRs have been boosted by a factor of $(1+z)^{0.6}$ to produce more star formation at high redshift (Eq. 2; also see Fig. 8 of Cattaneo et al. 2006 for the impact of this assumption on the evolution of the cosmic SFR density). While this assumption increases the stream-fed SFR, the factor $(1+z)^{0.6}$ has been assumed to multiply both the disc SFR and the bulge SFR. Thus it does not change the relative importance of the two in terms of star formation efficiency.

The most serious concern is that our model may exaggerate gas consumption in protogalaxies at $z \gtrsim 4$, with the consequence that when the first major mergers occur, there is little gas left to trigger a starburst. To address this point, we have analysed the gas content of major mergers.

Fig. 11 is a remake of Fig. 3 where we only show the galaxies that have experienced a major merger in the last 300 Myr (the circled ones) and compare them to the merger-like objects observed in Tacconi et al., (2008). We colour-code the symbols according to their gas fraction. In GalICS, mergers of quenched, red-sequence galaxies are gas poor, but that is due to our quenching criterion, which is related to the critical halo mass M_{crit} , and has nothing to do with the star formation efficiency. So, let us focus on the galaxies that are on the main sequence of star forming galaxies.

In our model, at $z = 2$ and $M_* \lesssim 10^{10.5} M_\odot$, gas fractions range from ~ 0.3 to ~ 0.6 . There is a declining trend with mass, which is also observed (Tacconi et al. 2012). At $M_* \sim 10^{11} M_\odot$, the typical gas fraction is $\sim 0.15 - 0.2$, in agreement with the gas fractions of major mergers observed at $z = 2 - 3$ (Tacconi et al. 2008). Therefore, there is no reason to believe that we underestimate the importance of merger-driven star formation because the gas fractions of our mergers are systematically lower than they should be.

Our results are consistent with those that Cattaneo et al. (2011) obtained with a much simpler

galaxy formation model. In that article we concentrated on mass assembly (here we concentrate on star formation). We found that gas-rich mergers make a negligible contribution to the baryonic mass assembly of the overall galaxy population, although they contribute about half of the mass in ellipticals with $M_* < 10^{10.8} h^{-1} M_\odot$, which formed their stars at lower z than giant ellipticals due to downsizing (Thomas et al. 2005). Elliptical galaxies with $M_* > 10^{11} h^{-1} M_\odot$ accrete most of their mass via dry mergers. In Cattaneo et al. (2011), we did not consider the possibility that the critical mass above which gas accretion is shut down may be higher at higher redshifts and we wondered to what extent that could affect our conclusions. Here we have included a redshift dependence of M_{crit} (Eq. 1), but the basic picture has not changed.

Lowering z_{crit} , which is equivalent to increasing M_{crit} at high redshift, delays the shutdown of gas accretion but also transforms a number of dry mergers into wet mergers. The total amount of star formation increases but the relative importance of the two modes is almost unchanged. Values of z_{crit} substantially lower than $z \sim 3$ cause GALICS to overpredict the galaxy luminosity function at $z = 0$. This effect can be partially compensated by lowering the value of M_{crit} at $z = 0$ but there is limited leeway to do so.

In conclusion, the parameters of our model contain great uncertainties (particularly those anchored to the luminosity function of Lyman-break galaxies), which affect our capacity to trust the model's predictions in quantitative detail, especially since we know that it fails to reproduce the SFR- M_* relation inferred from observations at $z \sim 1 - 4$.

However, the basic results of our model are quite robust to changes in parameter values and model assumptions because it is difficult to increase the importance of wet mergers without also increasing the importance of stream-fed star formation, unless one finds a way to accrete large masses of gas while preventing them from making stars until the first mergers occur. These results corroborate the scenario portrayed by Dekel et al. (2009), where they made a distinction between the overall SFG population and extreme SMGs, which are about ten times less numerous. They conclude that the accretion of cold gas is the main mode of galaxy formation in the former population, whereas mergers are only necessary to explain the latter.

REFERENCES

- Barnes J. E., Hernquist L., 1996, *ApJ*, 471, 115
 Barnes J. E., Hernquist L. E., 1991, *ApJL*, 370, L65
 Baugh C. M., Lacey C. G., Frenk C. S., Granato G. L., Silva L., Bressan A., Benson A. J., Cole S., 2005, *MNRAS*, 356, 1191
 Bell E. F., McIntosh D. H., Katz N., Weinberg M. D., 2003, *ApJS*, 149, 289
 Binney J., Tremaine S., 2008, *Galactic Dynamics: Second Edition*. Princeton University Press
 Brown M. J. I., Dey A., Jannuzi B. T., Brand K., Benson A. J., Brodwin M., Croton D. J., Eisenhardt P. R., 2007, *ApJ*, 654, 858
 Cattaneo A., Dekel A., Devriendt J., Guiderdoni B., Blaizot J., 2006, *MNRAS*, pp 780–
 Cattaneo A., Dekel A., Faber S. M., Guiderdoni B., 2008, *MNRAS*, 389, 567
 Cattaneo A., Faber S. M., Binney J., Dekel A., Kormendy J., Mushotzky R., Babul A., Best P. N., Brüggen M., Fabian A. C., Frenk C. S., Khalatyan A., Netzer H., Mahdavi A., Silk J., Steinmetz M., Wisotzki L., 2009, *Nature*, 460, 213
 Cattaneo A., Mamon G. A., Warnick K., Knebe A., 2011, *A&A*, 533, A5
 Chen Y.-M., Wild V., Kauffmann G., Blaizot J., Davis M., Noeske K., Wang J.-M., Willmer C., 2009, *MNRAS*, 393, 406
 Cole S., Lacey C. G., Baugh C. M., Frenk C. S., 2000, *MNRAS*, 319, 168
 Conroy C., Wechsler R. H., 2009, *ApJ*, 696, 620
 Cox T. J., Dutta S. N., Di Matteo T., Hernquist L., Hopkins P. F., Robertson B., Springel V., 2006, *ApJ*, 650, 791
 Cresci G., Hicks E. K. S., Genzel R., Schreiber N. M. F., Davies R., Bouché N., Buschkamp P., Genel S., Shapiro K., Tacconi L., Sommer-Larsen J., 2009, *ApJ*, 697, 115
 Daddi E., Dickinson M., Morrison G., Chary R., Cimatti A., Elbaz D., Frayer D., Renzini A., Pope A., Alexander D. M., Bauer F. E., Gialavisco M., Huynh M., Kurk J., Mignoli M., 2007, *ApJ*, 670, 156
 Davis M., Efstathiou G., Frenk C. S., White S. D. M., 1985, *ApJ*, 292, 371
 De Lucia G., Blaizot J., 2007, *MNRAS*, 375, 2
 Dekel A., Birnboim Y., 2006, pre-print astro-ph/0412300
 Dekel A., Birnboim Y., 2008, *MNRAS*, 383, 119
 Dekel A., Birnboim Y., Engel G., Freundlich J., Goerdt T., Mumcuoglu M., Neistein E., Pichon C., Teyssier R., Zinger E., 2009, *Nature*, 457, 451
 Dekel A., Sari R., Ceverino D., 2009, *ApJ*, 703, 785
 Dekel A., Silk J., 1986, *ApJ*, 303, 39
 Eales S., Lilly S., Gear W., Dunne L., Bond J. R., Hammer F., Le Fèvre O., Crampton D., 1999, *ApJ*, 515, 518
 Elbaz D., Daddi E., Le Borgne D., Dickinson M., Alexander D. M., Chary R.-R., Starck J.-L., Brandt W. N., Kitzbichler M., MacDonald E., Nonino M., Popesso P., Stern D., Vanzella E., 2007, *A&A*, 468, 33
 Elbaz D., Dickinson M., Hwang H. S., Díaz-Santos T., Magdis G., Magnelli B., Le Borgne D., Galliano F., 2011, *A&A*, 533, A119
 Elmegreen B. G., Bournaud F., Elmegreen D. M., 2008, *ApJ*, 688, 67
 Engel H., Tacconi L. J., Davies R. I., Neri R., Smail I., Chapman S. C., Genzel R., Cox P., Greve T. R., Ivison R. J., Blain A., Bertoldi F., Omont A., 2010, *ApJ*, 724, 233
 Erb D. K., Steidel C. C., Shapley A. E., Pettini M., Adelberger K. L., 2004, *ApJ*, 612, 122
 Fardal M. A., Katz N., Weinberg D. H., Davé R., 2007, *MNRAS*, 379, 985
 Förster Schreiber N. M., Genzel R., Bouché N., Cresci G., Davies R., Buschkamp P., Shapiro K., Tacconi L. J., Hicks E. K. S., 2009, *ApJ*, 706, 1364
 Förster Schreiber N. M., Genzel R., Lehnert M. D., Bouché N., Verma A., Erb D. K., Shapley A. E., Steidel C. C., Davies R., Lutz D., 2006, *ApJ*, 645, 1062
 Genel S., Dekel A., Cacciato M., 2012, *ArXiv e-prints*
 Gonzalez V., Bouwens R., Ilingworth G., Labbe I., Oesch P., Franx M., Magee D., 2012, *ArXiv e-prints*

- Governato F., Brook C., Mayer L., Brooks A., Rhee G., Wadsley J., Jonsson P., Willman B., Stinson G., Quinn T., Madau P., 2010, *Nature*, 463, 203
- Guedes J., Callegari S., Madau P., Mayer L., 2011, *ApJ*, 742, 76
- Guiderdoni B., Hivon E., Bouchet F. R., Maffei B., 1998, *MNRAS*, 295, 877
- Hatton S., Devriendt J. E. G., Ninin S., Bouchet F. R., Guiderdoni B., Vibert D., 2003, *MNRAS*, 343, 75
- Hernquist L., 1990, *ApJ*, 356, 359
- Hopkins P. F., Hernquist L., Cox T. J., Di Matteo T., Robertson B., Springel V., 2006, *ApJS*, 163, 1
- Huang J.-S., Faber S. M., Daddi E., Laird E. S., Lai K., Omont A., Wu Y., Younger J. D., Bundy K., Cattaneo A., Chapman S. C., Conselice C. J., Dickinson M., Egami E., Fazio G. G., 2009, *ApJ*, 700, 183
- Kartaltepe J. S., Dickinson M., Alexander D. M., Bell E. F., Dahlen T., Elbaz D., Faber S. M., Lotz J., McIntosh D. H., Wiklind T., Altieri B., Aussel H., Bethermin M., Bournaud F., Charmandaris V., 2011, *ArXiv e-prints*
- Kereš D., Katz N., Weinberg D. H., Davé R., 2005, *MNRAS*, 363, 2
- Khochfar S., Ostriker J. P., 2008, *ApJ*, 680, 54
- Kitzbichler M. G., White S. D. M., 2007, *MNRAS*, 376, 2
- Krumholz M. R., Dekel A., 2012, *ApJ*, 753, 16
- Krumholz M. R., Dekel A., McKee C. F., 2012, *ApJ*, 745, 69
- Lacey C. G., Baugh C. M., Frenk C. S., Silva L., Granato G. L., Bressan A., 2008, *MNRAS*, 385, 1155
- Magdis G. E., Rigopoulou D., Huang J.-S., Fazio G. G., 2010, *MNRAS*, 401, 1521
- Martig M., Bournaud F., Teyssier R., Dekel A., 2009, *ApJ*, 707, 250
- McCarthy I. G., Schaye J., Font A. S., Theuns T., Frenk C. S., Crain R. A., Dalla Vecchia C., 2012, *ArXiv e-prints*
- Mihos J. C., Hernquist L., 1994, *ApJL*, 425, L13
- Mihos J. C., Hernquist L., 1996, *ApJ*, 464, 641
- Noeske K. G., et al., 2007a, *ApJL*, 660, L47
- Noeske K. G., et al., 2007b, *ApJL*, 660, L43
- Ostriker J. P., 1980, *Comments on Astrophysics*, 8, 177
- Piontek F., Steinmetz M., 2011, *MNRAS*, 410, 2625
- Reddy N. A., Pettini M., Steidel C. C., Shapley A. E., Erb D. K., Law D. R., 2012, *ApJ*, 754, 25
- Rodighiero G., Cimatti A., Gruppioni C., Popesso P., Andreani P., Altieri B., Aussel H., Berta S., Bongiovanni A., Brisbin D., Cava A., Cepa J., Daddi E., Dominguez-Sanchez H., Elbaz D., 2010, *A&A*, 518, L25
- Sanders D. B., Scoville N. Z., Young J. S., Soifer B. T., Schloerb F. P., Rice W. L., Danielson G. E., 1986, *ApJL*, 305, L45
- Santini P., Fontana A., Grazian A., Salimbeni S., Fiore F., Fontanot F., Boutsia K., Castellano M., Cristiani S., de Santis C., Gallozzi S., Giallongo E., Menci N., Nonino M., Paris D., Pentericci L., Vanzella E., 2009, *A&A*, 504, 751
- Smail I., Ivison R. J., Blain A. W., 1997, *ApJL*, 490, L5+
- Somerville R. S., Primack J. R., 1999, *MNRAS*, 310, 1087
- Springel V., Di Matteo T., Hernquist L., 2005, *MNRAS*, 361, 776
- Stark D. P., Ellis R. S., Bunker A., Bundy K., Targett T., Benson A., Lacy M., 2009, *ApJ*, 697, 1493
- Tacconi L. J., Genzel R., Smail I., Neri R., Chapman S. C., Ivison R. J., Blain A., Cox P., Omont A., Bertoldi F., Greve T., Förster Schreiber N. M., 2008, *ApJ*, 680, 246
- Thomas D., Maraston C., Bender R., Mendes de Oliveira C., 2005, *ApJ*, 621, 673
- Toomre A., 1964, *ApJ*, 139, 1217
- Toomre A., Toomre J., 1972, *ApJ*, 178, 623
- Treyer M., Schiminovich D., Johnson B., Seibert M., Wyder T., Barlow T. A., Conrow T., Forster K., Friedman P. G., Martin D. C., Morrissey P., Neff S. G., Small T., Bianchi L., Donas J., 2007, *ApJS*, 173, 256
- van den Bosch F. C., 1998, *ApJ*, 507, 601
- Wuyts S., Förster Schreiber N. M., Lutz D., Nordon R., Berta S., Altieri B., Andreani P., Aussel H., Bongiovanni A., Cepa J., Cimatti A., Daddi E., Elbaz D., Genzel R., Koekemoer A. M., 2011, *ApJ*, 738, 106